Materials Today Chemistry 23 (2022) 100682

Contents lists available at ScienceDirect

Materials Today Chemistry

journal homepage: www.journals.elsevier.com/materials-today-chemistry/

Morphological aspects determine the catalytic activity of porous hydrocalumites: the role of the sacrificial templates

S. Muráth [a, b], T. Varga [c], Á. Kukovecz [c], Z. Kónya [c, d], P. Sipos [e, f], I. Pálinkó [e, g, h], G. Varga [a, e, *]

[a] Department of Physical Chemistry and Materials Science, University of Szeged, Rerrich Béla Tér 1, Szeged, H-6720, Hungary
[b] MTA-SZTE "Lendület" Biocolloids Research Group, Institute of Chemistry, University of Szeged, Aradi Vértanúk Tere 1, Szeged, H-6720, Hungary
[c] Department of Applied and Environmental Chemistry, University of Szeged, Rerrich Béla Tér 1, Szeged, H-6720, Hungary
[d] MTA-SZTE Reaction Kinetics and Surface Chemistry Research Group, Rerrich Béla Tér 1, Szeged, H-6720, Hungary
[e] Materials and Solution Structure Research Group, and Interdisciplinary Excellence Centre, Institute of Chemistry, University of Szeged, Aradi Vértanúk Tere 1, Szeged, H-6720, Hungary
[f] Department of Inorganic and Analytical Chemistry, University of Szeged, Dóm Tér 7, Szeged, H-6720, Hungary
[g] Department of Organic Chemistry, University of Szeged, Dóm Tér 8, Szeged, H-6720, Hungary

ARTICLE INFO

Article history:
Received 2 August 2021
Received in revised form
8 November 2021
Accepted 9 November 2021
Available online xxx

Keywords:
Micropore-mesopore architectures
Surface-engineered porous LDHs
Sacrificial template method
Knoevenagel condensation
Pore structure–catalytic activity relationships

ABSTRACT

Morphological modification of bulk layered double hydroxides (LDHs) into surface-engineered, porous materials enabled effective, base-catalyzed liquid phase Knoevenagel condensation in water. The increase in the number of the accessible basic sites on LDH engineering led to the enhancement of the reaction rate, whereas the significant changes in the relative strength of the basic sites were found to cause remarkable differences in the chemoselectivities. Thus, porous hydrocalumite (CaAl-LDH) catalysts allowed long-term and highly selective Knoevenagel condensation using reasonably mild reaction conditions. The advantages of heterogeneous nature and the recyclability of the hydrocalumites were also strengthened by advanced surface treatment. These key factors (basic sites, basic nature, and heterogeneity) can be fine-tuned by selecting the appropriate sacrificial template (cetyl trimethyl ammonium bromide, multiwalled carbon nanotubes, and Santa Barbara Amorphous-15), which regulates the morphology of the composites.

1. Introduction

Liquid phase Knoevenagel condensation reaction of aldehydes/ketones with compounds of activated methylene groups is a key process to produce a variety of intermediates and fine chemicals such as substituted alkenes [1,2], therapeutic drugs [3,4], and functional polymers [5,6] for various industrial synthetic processes. Condensation catalysts are generally based on soluble Brønsted bases [7–9] and have been applied widely in industries. In spite of their well-known disadvantages such as unsatisfactory yields, circuitous (or often impossible) reusability, harsh reaction conditions, and high-cost implications, these catalysts are still in use in most Knoevenagel condensation reactions.

The application of insoluble Brønsted bases/Lewis acids appeared to be the most promising alternative of avoiding undesirable impacts associated with the application of homogeneous catalysts. In the last few decades, numerous studies have focused on using zeolites [10–15], zeo-type compounds [16–18], layered double hydroxides (LDHs) [19–22], oxides, and mixed oxides of alkaline earth metals and clay minerals (Table S1) as catalysts [23–29]. Despite their undisputable advantages such as their strong and tunable basicity/acidity, high specific surface area, and unique porosity, the results fell behind expectations. This was largely owing to the relatively narrow range of reaction conditions that are necessary to be applied to achieve the desired efficiency. In particular, selective operation of these heterogeneous catalysts was strongly limited to (i) high reaction temperatures (130–180 °C), (ii) environmentally 'unfriendly' solvents (aldehydes, dimethylformamide [DMF], and benzene), (iii) the necessity of relatively large amounts of added catalysts (10–20 mol%), and (iv) the need of using inert atmosphere [30]. In addition to these, deactivation or

* Corresponding author.
E-mail address: gabor.varga5@chem.u-szeged.hu (G. Varga).
[h] Deceased.

https://doi.org/10.1016/j.mtchem.2021.100682

thermal/chemical instability, associated with structural properties of these catalysts, is also to be considered serious limiting factors. Overall, the previously obtained results in the field indicated that the number of accessible active sites and the development of their porous structure are closely linked to the diffusion of the reactants and products, which are the main factors to maximize efficiency.

Although notable progress in environmentally friendly condensation catalysts has been achieved with, for example nanoparticles and functional materials (Table S1) [30], particularly, 2D materials [31–34], nanocomposites [35,36] as well as metal-organic frameworks (MOFs) [37–40] or carbon nitrides [41–43] and ionic liquids [44–46] etc., these proved to be unmanageable catalysts because of practical reasons [30]. It is necessary to establish specific conditions for their intended uses with regard to their synthesis and handling. A further important aspect is the cost of these systems, which considerably exceeds the usual price expected for commercial catalysts.

These concerns motivated researchers to look for environmentally friendly catalysts based on commercial solid bases (Table S1). Hydrotalcites (HTs), an important class of LDHs, are well-studied and promising solid bases in various catalytic reactions; however, they present some severe limitations toward selective Knoevenagel condensations (Table S1) [27,47,48]. Besides their low-controllable basic sites, the diffusion limitations must be considered as a result of their low external surface areas and smaller abundance of available basic sites; these are the major drawbacks of HTs as catalysts. Considering these facts, the lack of porous counterparts of HTs as actual catalysts for condensations is very surprising. This can be partially explained by the fact that only a few synthetic strategies have been developed to produce template-free LDHs with well-controlled pore structure [49]. Moreover, most of these composites possessed microporous or macroporous structures [50–52] that have less relevance in catalytic applications (Table S2) [53]. Adding to this, that the complete removal of the template is essential for producing effective solid base catalysts, otherwise, the basic sites remain at least partially hindered [54,55].

Some previously applied templates such as multiwalled carbon nanotubes (MWCNTs) [56] and mesoporous Santa Barbara Amorphous silica (SBA-15) [57–59] and cetyl trimethyl ammonium bromide (CTAB) [60,61] seem to be removable to form mesoporous or microporous-mesoporous structures. The role of the templates was systematically studied during the formation of LDH-based composites. For instance, notable effects on the crystallization of HTs were observed and led to significant morphological changes [57,58]. By using CNTs or zeolites as templates, growth of highly dispersed LDH nanocrystals on the surface of CNTs [56] or vertically aligned LDH on zeolites have already been reported [58]. Besides, using CTAB gave rise to the formation of composites with horizontally stacked LDH lamellae [61]. However, owing to the limited information on the syntheses of template-free porous LDHs, a well-established relationship between the morphology of the template-containing composites and the pore structure of porous (template-free) LDHs thus obtained is still unknown.

From the catalysis point of view, limited attention has been paid to the members of the hydrocalumite (HC) supergroup of LDH, such as CaAl–LDH [19], that have more advantageous basic character and external surface area compared with HTs [62,63].

In the current contribution, alternative synthetic routes based on using three conventional templates (MWCNT, SBA-15, CTAB) and a water-based sol-gel synthesis strategy for template-free porous HCs/HTs with controlled pore structure are presented (Scheme 1). Particular attention was paid to the morphological effect of the template-loaded composites on the porosity of the designed product. The results of using porous and commercial LDH analogs as actual catalysts in Knoevenagel condensations are presented. They include (I) effective condensations in water under ambient conditions using HCs, (II) selective condensations with an enhanced reaction rate by porous LDHs, and (III) detailed porosity-basicity-activity-stability relationship with insights into the impact of pore size as well as accessible basic sites in condensations.

2. Experimental part

2.1. Materials

All the analytical reagent (AR) chemical reagents were purchased from Merck and Sigma-Aldrich and used as received without further purification.

2.2. Synthesis of the LDH composites

The template-free (reference) CaAl-LDH (denoted as HC from hydrocalumite) was synthesized by a simple sol-gel method based on our previous study. Accordingly, a 2:1 M ratio mixture of Ca-methoxide (67 mmol) and Al-ethoxide (33 mmol) was prepared in 50 mL of distilled water and was stirred with a portion (20 mmol) of $NaNO_3$ for 12 h [64]. The suspension was filtered, washed with water several times, and dried for 24 h at 60 °C. The reference MgAl-LDH (denoted as HT from hydrotalcite) was prepared by the same method, but using a 3:1 Mg:Al molar ratio (with 75 mmol of Mg ethoxide). Heat-treated LDHs were prepared from the HC and HT at 450 °C for 12 h (denoted as calc-HC and calc-HT). To rehydrate these ones, a slurry phase reconstruction method was used. An appropriate portion of calc-HC/calc-HT (~0.5 g) was suspended in a 100 mL solution mixture (H_2O/EtOH/0.015 M NaOH of 85:5:10 vol ratio) in which 20 mmol $NaNO_3$ was also dissolved to provide interlayer nitrate ions. The obtained slurries were rigorously stirred for 96 h at 50 °C followed by filtration, washed with water and ethanol several times, and dried for 24 h at 60 °C in an oven. The solid products were denoted as recon-HC/recon-HT (recon stands for reconstructed).

The LDHs containing various templates were prepared by using the previously mentioned sol-gel method with the following modifications. In a typical method, 50 mL aqueous solution of a mixture of calcium or magnesium alkoxide and aluminum ethoxide in 2:1 and 3:1 M ratio, respectively, (total metal content was 50 mmol) as well as 10 mmol of $NaNO_3$ was added to 50 mL ultrasonicated ethanolic suspension of MWCNTs (0.5 g) [56] or SBA-15 (0.5 g) [57] under vigorous stirring at room temperature. The resulting materials (denoted as M-HC/S-HC or M-HT/S-HT, where M stands for MWCNTs and S for SBA-15), after aging for 96 h at 60 °C, were filtered, washed with 1:1 ratio of ethanol/water mixture several times, and dried at 60 °C overnight.

During the construction of LDHs with well-defined pore structure, the obtained M-HC/M-HT composite samples were calcined at 550 °C for 48 h to remove the MWCNT template (denoted as calc-M-HC/calc-M-HT). The LDH structures were reconstructed by the same rehydration procedure described above to obtain the recon-M-HC/recon-M-HT. SBA-15 was also completely removed by stirring it in a 2 M aqueous NaOH solution at 60 °C followed by several washing steps with water (calc-S-HC/calc-S-HT), stirring for regeneration with nitrate-containing (20 mmol) aqueous solution, filtering, and a final drying step at 60 °C to obtain the recon-S-HC/recon-S-HT.

For production of CTAB-LDH composites (C-HC/C-HT; C stands for CTAB), 50 mL aqueous solution of CTAB (40 mmol, corresponds to a concentration above the critical micellar concentration) [61] was prepared. Apart from using an aqueous solution of the template, a method identical to that described above was applied. The CTAB was removed by calcination at 510 °C for 16 h (calc-C-HC/calc-

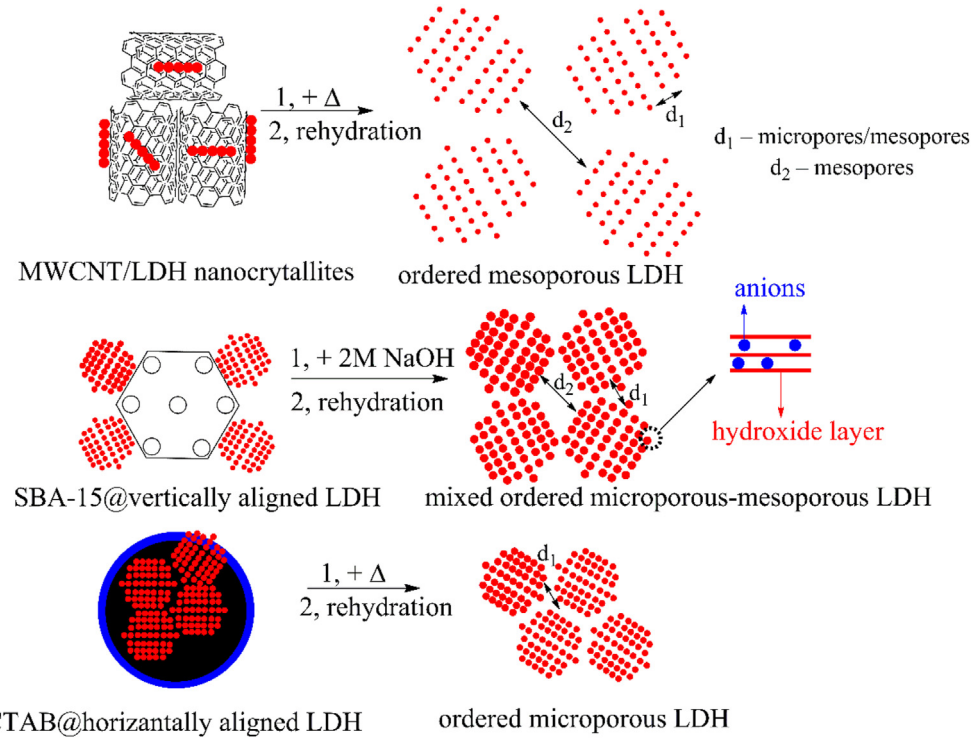

Scheme 1. Schematic procedure for the preparation of template-free, ordered porous layered double hydroxides (LDHs).

C-HT) followed by a rehydration step similar to those of the HC/HT composites to obtain the final products (denoted as recon-C-HC or recon-C-HT).

2.3. Characterization methods

X-ray diffractograms were recorded on a Rigaku XRD-MiniFlex II instrument using CuKα radiation (λ = 0.15418 nm), 40 kV accelerating voltage at 30 mA. The diffraction patterns were evaluated by using the DICVOL-06 routine included in the Expo2013 package to offer the crystal parameters [62]. Scanning electron microscopy (SEM) images were taken by using an S-4700 scanning electron microscope (SEM, Hitachi, Japan) with an accelerating voltage of 10–18 kV to study the morphologies of the samples. Spatially better-resolved images were recorded by transmission electron microscopy (TEM). For this, a FEI Tecnai G^2 20 X-Twin type instrument operating at an acceleration voltage of 200 kV was used.

For the characterization of the framework and interlayer anions, a large variety of experimental means were applied. FT-IR spectra were recorded on a BIO-RAD Digilab Division FTS-65A/896 apparatus equipped with ATR or GIRA (grazing incidence reflection absorption) accessories to reveal the depth profile of the composites. GIRA-FTIR technique with an incidence angle ranging from 75 to 88° can be a useful tool for characterizing the surface area [65], whereas ATR spectroscopy can be suitable for identifying the bulk species. For each spectrum, 256 scans were collected with 4 cm^{-1} resolution, and the range of 4000–600 cm^{-1} was registered. For GIRA spectra, LDH film from an alcoholic suspension was deposited on ZnSe 45° trapezoidal-shaped crystals and was measured in a variable angle cell with an incidence angle of 80°. Raman spectra were obtained on a Thermo Scientific™ DXR™ Raman microscope at an excitation wavelength of 720 nm applying 10 mW laser power and averaging 20 spectra with an exposition time of 6 s.

Porosity and surface area studies were performed on a NOVA3000 instrument (Quantachrome, USA) gas adsorption system using nitrogen as the adsorbate. All the samples were outgassed under vacuum for 16 h at 25 °C before adsorption measurements. Surface areas were calculated using the Barrett–Joyner–Halenda (BJH) method in the 0.05–0.35 relative pressure range.

The ratio of metal the ions was determined using a Perkin Elmer Optima 7000DV inductively coupled plasma optical emission (ICP–OES) spectrometer. Yttrium internal standard was used for the measurements. For sample preparation, an accurately known amount (a few milligrams) of the solid materials was dissolved in 5 mL of cc. HCl. After dissolution, the samples were diluted with distilled water to 100 mL and filtered.

Electrophoretic mobility values were measured using an Anton Paar LiteSizer 500 device equipped with a 40 mW laser source operating at 658 nm wavelength. Omega-shaped plastic capillary cuvettes (Anton Paar) were used for the electrophoretic experiments, and surface charge densities were determined (detailed in the Supplementary Information). Hydrodynamic radii were measured by dynamic light scattering (DLS) using the same instrument. The cumulative method was applied to fit the correlation functions, which were collected for 20 s. Data collection was conducted at 175° scattering angle at 25 °C. The particle doses (25 mg/L, i.e. 25 ppm) were the same for both the electrophoretic and the DLS experiments, whereas the pH was kept at 7.

The basicity of the samples was characterized by Brønsted basicity titrations. For these experiments, 50 mg of the sample were then suspended in a solution mixture of 20 mL methanol, and 0.5 mL of a 0.2% indicator solution containing bromothymol blue (pK_a = 7.1), phenolphthalein (pK_a = 9.3), and indigo carmine (pKa = 12.2) in methanol was also added. Thereafter, the solution was titrated against benzoic acid (0.01 M), while stirring continuously at 500 rpm [66]. The basic sites were also characterized by CO_2-temperature programmed desorption (TPD) technique. TPD measurements were performed on a Hewlett-Packard 5890 GC system equipped with a TCD detector. Before the measurements, a

quartz tube was loaded with a portion of the sample (100 mg) followed by the first purge in a flow of He (50 mL/min) at room temperature for 10 min to remove impurities. After that, using the 10 °C/min ramp rate, the temperature was increased to 450 °C and was then kept for 1 h to remove water and any other impurities. Subsequently, the temperature was decreased to 100 °C. Finally, the gas was changed to CO_2 in He (30 mL/min CO_2, 50 mL/min He) and circulated over the sample for 1 h.

The thermal behavior of the HCs was studied by thermogravimetry (TG) and differential thermogravimetry (DTG). The samples were studied with a Setaram Labsys derivatograph operating in air at a 5 °C min^{-1} heating rate. For the measurements, 20–30 mg of the samples were applied.

2.4. General procedure for the catalytic reactions

Samples containing benzaldehyde (10.0 mmol) and ethyl acetoacetate or malononitrile (15.0 mmol) (or other compounds with active methylene group[s]) with solid LDH as catalysts (0.1 g) as well as with 3.0 mL of water as solvent were magnetically stirred while keeping the reaction temperature at 50 °C under N_2 atmosphere. A portion of the reaction mixture was quenched after 5–120 min with 6 M ice-cold HCl solution. The product was extracted with ethyl acetate (3 × 10 mL). The combined organic extracts were dried using anhydrous sodium sulfate, evaporated under reduced pressure, and assayed on a Hewlett-Packard 5890 gas chromatograph equipped with Agilent-1 column and a flame ionization detector, using internal standard (dodecane) method. The products were identified using authentic samples.

To identify the condensation products, NMR spectra were also recorded (listed in the Supporting Information, S3. section) using a Bruker DRX500 NMR instrument operating at 500 MHz. All samples were dissolved in 0.7 mL DMSO-d_6, and ^{1}H–NMR and ^{13}C–NMR spectra were recorded at room temperature. Spectra were referenced internally to the remaining resonance of the DMSO-d_6 at 8.26 ppm.

3. Results and discussion

3.1. Morphological changes of the parent LDHs

The solid samples were characterized by XRD first. As can be seen in Fig. 1 and Fig. S1., the isolated products showed distinct XRD patterns which were identified as typical Bragg reflections of the corresponding HTs (PDF# 89–5434) or HCs (PDF# 89–6723) without the appearance of any other crystalline phases [67–70]. Minor variations in the lattice constants and dimensions of the as-prepared LDHs were observed compared with the conventional samples with rhombohedral crystal symmetry (Table S3) This is owing mainly to the changes in the hydration of the interlamellar space, resulting in a decrease of the interlayer distances. Furthermore, relevant broadening of the characteristic reflections for SBA-15-containing composites was found, similar observations were made for zeo-type–LDH composites [58]. Besides, a second LDH phase with somewhat smaller interlayer distance appeared in the case of CTAB-containing composite. Furthermore, the used templates did not have any characteristic reflections in the 2θ range studied, except for MWCNTs: this Bragg reflection was indexed to [002] and was observed at about 26° 2θ (PDF# 89–8487) [71] confirming the existence of MWCNTs with a d-spacing of 0.34 nm.

The morphological changes of HCs on using different templates were investigated by combining TEM and SEM microscopies (Fig. 2; Fig. S2. for HTs). In contrary to the well-known hexagonally shaped 2D morphology with stone-like crystallites of the commercial samples [72], large variations were observed in the crystal shape for

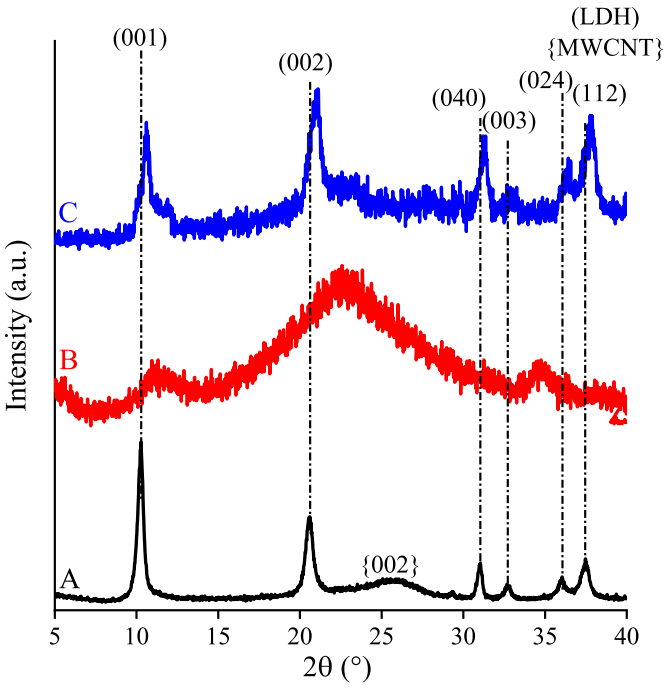

Fig. 1. XRD patterns of M–HC (**A**); S-HC (**B**), and C-HC (**C**).

composite materials. In the case of M-HC/M-HT, besides species with filamentous morphology in the images attested to the integration of MWCNTs [56], the considerable number of LDH nucleus with significantly decreased crystallite size — compared with commercial samples — can be seen that were ordered on the surface of MWCNTs [73]. A portion of these crystallites seemed to be separated from the surface of the template and exhibited close fit to the adsorbed LDHs producing altogether insular clusters [56]. On repeating the synthesis with the presence of SBA-15 as templates, TEM and SEM images revealed well-known rosette-shaped aggregates that were built up around LDH nanosheets on the surface of the template. The formation of a core-shell composite can be implied from this observation. It was found that LDH nanoplates with smooth edges and with large particle size grew vertically on the core support constructing a shell with a thickness of *ca.* 250 nm, which are in line with previously reported results [57].

Microscopy images of C-HC showed that large clusters of irregular shape were formed suggesting the estimate of core-shell hybrids in which LDH platelets are horizontally aligned with the positively charged surfactant.

To fully ascertain the presence of the SBA-15/CTAB templates in our solids, a set of spectroscopic measurements was carried out. ATR-IR spectra are presented in Fig. 3, Figs. S3. and S4. Characteristic broad bands were detected for the S-HC and C-HC composites in the range of 1850–1200 cm^{-1}, and they originate from the LDH-shell (Table S4) [74–76]. Besides, the bands in the range of 1200–800 cm^{-1} belong to the templates. In particular, the asymmetric stretching of Si–O–Si unites (1017 cm^{-1}) related to SBA-15 framework [77] and the stretching mode vibration of C–N^+ moiety (980 cm^{-1}) for CTAB-containing sample [60], were identified. Moreover, in the latter case, the characteristic bands at 2916 and 2851 cm^{-1} are assigned to the symmetric and asymmetric stretching of $-CH_2$ units in the CTAB chain (Fig. S4.) [60], confirming that the envisioned LDH-CTAB composite was produced.

To better support the formation of core-shell composites for C-HC and S-HC (Fig. 3./Fig. S4. for HT), a comparative IR study was carried out to identify surface species. The differences in the

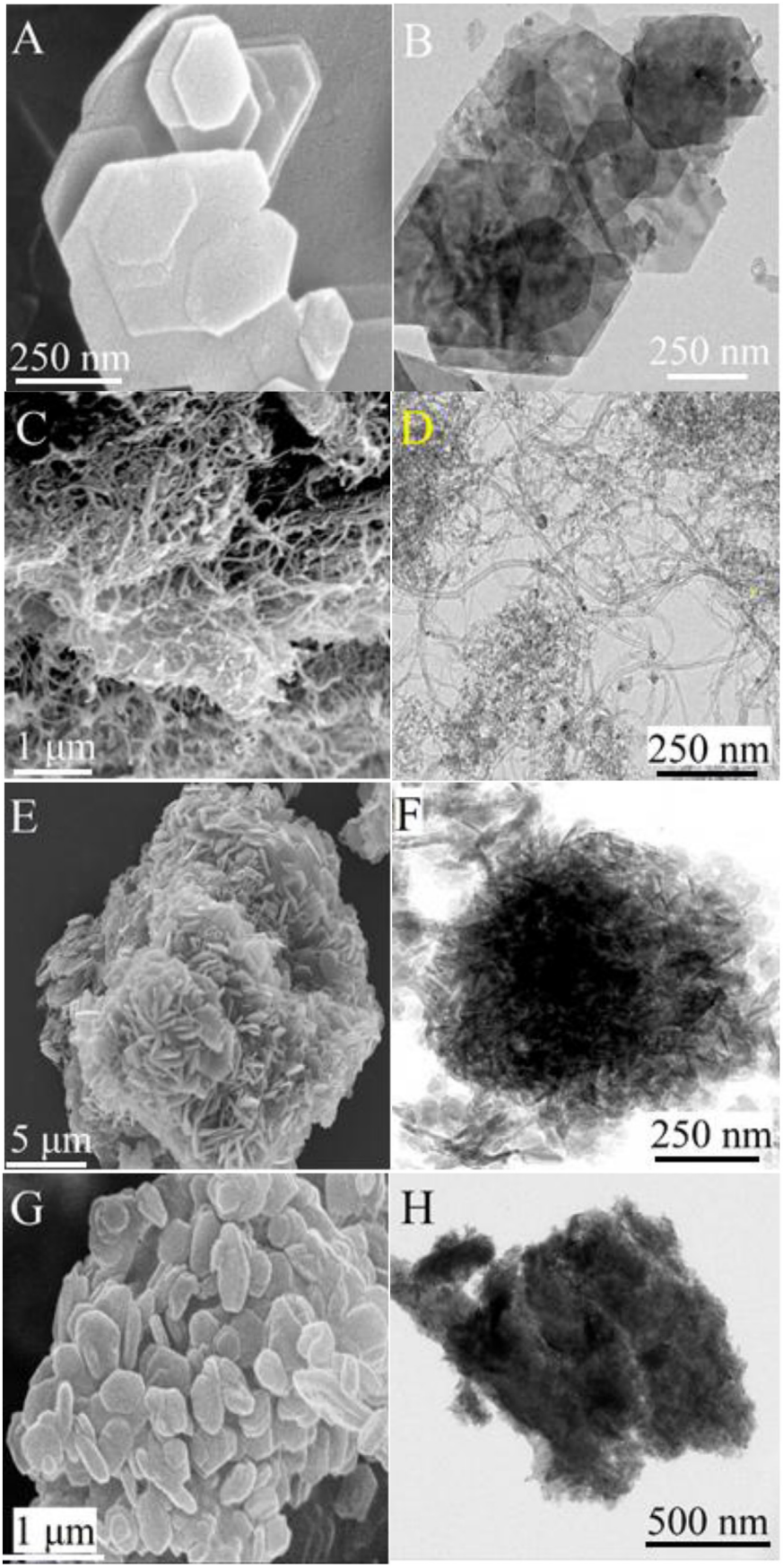

Fig. 2. SEM (**A; C; E; G**) and TEM images (**B; D; F; H**) of HC (**A; B**); M – HC (**C; D**); S-HC (**E; F**) and C-HC (**G; H**).

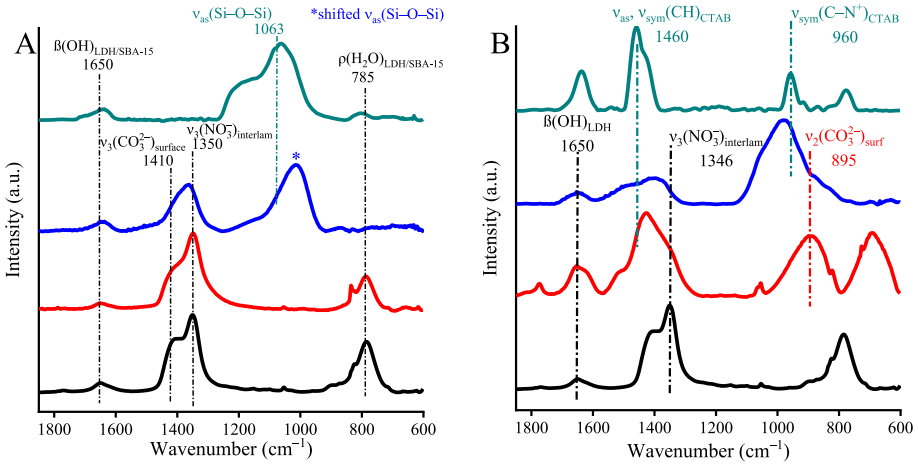

Fig. 3. ATR-IR spectra of HC (black), C-HC/S-HC samples (blue), and SBA-15/CTAB (green) as well as GIRA spectra of S-HC/C-HC (red). (**A**: SBA-15; **B**: CTAB).

penetration depth profile of the used methods (ATR and GIRA) provided the theoretical basis for such procedure. For both composites, the amount of characteristic bands of LDH and the templates could be recognized by ATR method, as described above. Contrarily, all vibrations originating from the templates are absent on using GIRA as surface-sensitive detection mode. This fact verifies that LDH shells have been formed during the synthesis in both cases. Moreover, the accumulation of carbonate ions on the surface could be determined by GIRA in the case of CTAB-loaded HC (Table S4) [78].

The presence of CTAB has also been proven by surface charge density determination. Although CaAl-LDH had negative surface charge (−6.5 mC/m^2, probably owing to the favored surface adsorption of airborne CO_2), CTAB-CaAl-LDH possessed +6.0 mC/m^2 surface charge density (Fig. S5.). This is possibly owing to electrostatic interactions between the LDH and CTAB which are in line with the previously reported findings [61,79].

Overall, the formation of composite materials with the designed morphology could be observed. One can note that using MWCNT/SBA-15/CTAB templates, a very simple and cost-effective sol-gel method was developed.

With the developed composites in our hands, the removal of the templates and reconstruction steps for creating porous LDH structure was attempted. A combination of XRD and various vibrational spectroscopic methods has been applied to monitor the synthetic procedures. Representative XRD analysis of the treated and rehydrated M – HC samples is presented in Fig. 4. (the remaining ones can be seen in Fig. S6.). After eliminating the template, a mixed oxide phase remained, as confirmed by XRD patterns analogous to the ones reported earlier for LDO phases [76]. Then, as a result of a simple rehydration process, phase pure, well-crystallized product could be solidified without any doubt. The crystal parameters of the final products calculated are consistent with those ones given for the composites (Table S3).

To further confirm the success of the template removal, vibrational spectroscopic methods were used. Because the MWCNT exhibits well-known fingerprint-like shifts in the middle of the usual FT-IR wavenumber region, its disappearance was justified by Raman spectroscopy (Fig. 4./Fig. S6.) [80]. Hence, D and G bands — in exactly the same positions as previously described — can be seen for the M – HC sample, whereas there are no similar Raman peaks either for the layered double oxides (LDO) or for its rehydrated counterpart. Accordingly, the used removal process was found to be sufficient to remove the MWCNT. One Raman shift shown was associated with nitrate anions [74] confirming the success of the incorporation of these anions during the rehydration. Removal of the other templates could be determined in a similar way using ATR-IR spectroscopy (Fig. S6.). For these products, similar

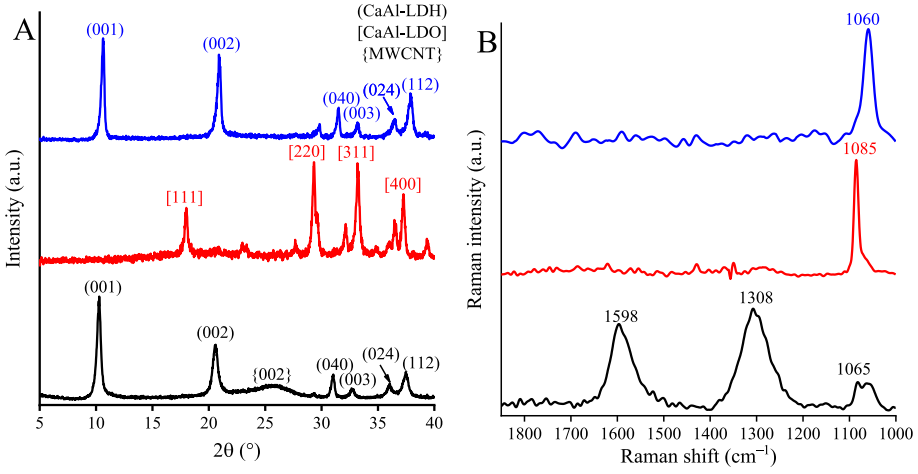

Fig. 4. XRD patterns (**A**) and Raman spectra (**B**) of M – HC (black); calc-M-HC (red) and recon-M-HC (blue).

statements could be made as for M-HC/recon-M-HC. After the rehydration, vibrational bands characteristic of LDH can be observed (1650, 1400, 1350, and 780 cm^{-1}) that closely resemble those identified for the nitrate-containing raw material.

A morphological summary of the template-free, rehydrated HCs is shown in Fig. 5. TEM images of recon-HCs (recon-HTs are represented in Fig. S7.) indicate the dependence of LDH morphology on the type of substrate. In particular, the MWCNT-based product consisted of nanoplates that grew uniformly in a vertical direction from each other. In addition, for recon-M-HC, mesoporous fringes of uniform widths can be clearly observed [81]. Alternatively, the product from LDH-SBA-15 composite has a notably diverse morphology, with thin sheet-like particles that are ordered to each other in non-*ab*-face stacking, thereby creating nest-like aggregates [82]. In addition, during the reorientation of the LDH particles on CTAB removal, most probably, *ab*-face stacking dominated again resulting in stone-like aggregates without any well-recognizable shape [83].

The specific surface areas were also found to be affected by the morphological changes, as shown by the results of the N_2-BET measurements (Table 1; Fig. S8., Table S5). The specific surface area significantly increased in the order of recon-M-HC > recon-S-HC > recon-C-HC » HC indicating the morphology response to the applied treatment. Slight variations in the measured dimensions for template-free final products were determined; however, significant changes were not observed (Table S3). Contrarily, both the total pore volume and the average pore diameter showed a significant dependence on the reaction conditions during the synthesis. It is important to see that the presented values notably increased. More precisely, up to 21-fold and 12-fold increases were detected in specific surface area and total pore volume, respectively, relative to the parent HC. The absolute values (310.2 m^2/g; 0.463 mL/g) indicate the synthesis of an advanced product compared with porous LDH reported previously (Table S2). Noticeably, by removing the templates used, slight increase in the actual molar ratio of Ca:Al metal centers was also ascertained. The extent of the variation is not significant; however, LDHs with a low number of defect sites would have superior efficiency in catalytic reactions as published previously [84,85]. Furthermore, template removal had also an impact on the thermal behavior of the template-free, as-prepared HC compared with pure CaAl-LDH. In particular, in the range between 25 and 125 °C, TG-DTG curves (Fig. S9.) displayed more significant mass losses for porous-like structures than the commercial ones. This can be correlated with enrichment in surface adsorbed water after the treatment of LDHs. In addition, for the modified structures, in the high-temperature range (500−700 °C), the losses owing to the decomposition of the lamellar structure occurred at lower temperatures. This finding is most probably owing to nitrous gases that are easy to remove because of the much larger surface areas created. In the case of the recon-S-HC sample, precise analysis cannot be performed because the characteristic mass losses largely overlapped. Taking into consideration the total mass loss of recon-S-HC, similar or exactly the same thermal behavior can be assumed as for, that is the recon-C-HC.

The BJH method provided details on the pore width distributions. In all cases, the desired products exhibited type IV isotherms with H3 hysteresis loop based on IUPAC classification (Fig. S8.,

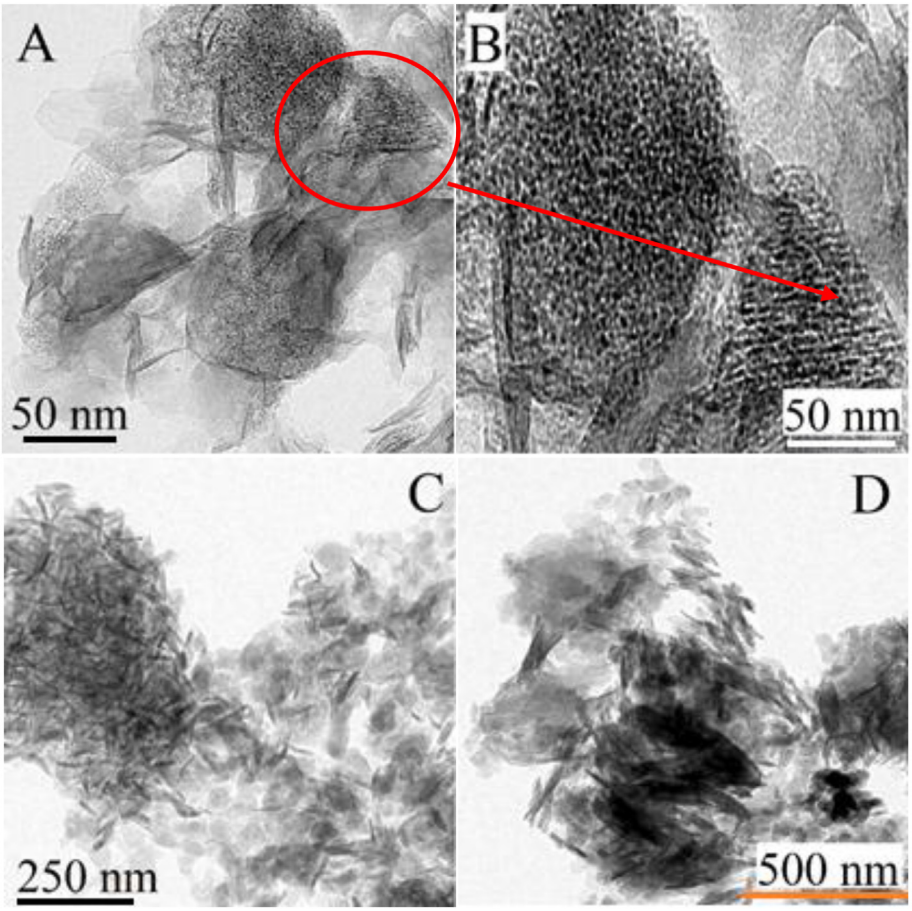

Fig. 5. TEM images of recon-M-HC (**A, B**); recon-S-HC (**C**), and recon-C-HC (**D**).

Table 1
Measured total pore volumes and specific surface areas as well as average pore diameters for the modified hydrocalumites.

Composites	Total pore volume (cm^3/g)	Surface area (m^2/g)	Average pore diameter (nm)	Ca:Al ratio[a]
HC	0.036	15.2	–	2.00
recon-HC	0.104	136.4	15.2 (meso)	2.05
recon-M-HC	0.463	310.2	4.0 (meso)	2.15
recon-S-HC	0.270	299.0	2.5 (meso) 1.6 (micro)	2.11
recon-C-HC	0.220	260.0	1.8 (micro)	2.07

[a] Detected by ICP-OES.

Table 1, Table S5) [57,76]. Some distortions in the loop structure can be detected confirming the differences in the ratio of micropores and the possible mesopores [86]. Most of all, the porosity of the HC/HT was substantially modified by using our envisioned sacrificial template-based syntheses (Fig. 6/Fig. S8.). By inhibiting aggregation of the primary LDH nanosheets led to the formation of ordered mixed pore structure (SBA-15; recon-S-HC) or a nanostructure with mesoporous-like character (MWCNT; recon-M-HC), having relatively narrow pore width distribution (4.0–16.0 nm) in the absence of the template. Only a few studies based on sacrificial template method were able to present similar results (Table S2) [76,87]. On the other hand, to the best of our knowledge, there has been no example for preparing HC with porous structure yet. In case of aggregation *via ab*-face stacking in the presence of the template (CTAB), an ordered microporous material with unprecedentedly unique pore diameter (1.8 nm) was obtained after the calcination-dehydration cycle. Therefore, the developed methods proved to be efficient for the creation of well-ordered porous LDH structures in a tunable manner. Furthermore, clear relationship between the morphology of the template-loaded structures and the pore structure of the emerging LDHs has been established.

3.2. Catalytic behavior of porous LDHs

For testing the catalytic properties, the base-catalyzed Knoevenagel condensation with various active methylene group-containing compounds (Scheme 2 — malononitrile) was chosen. For a comparison, owing to theoretical reasons, not only the pure LDHs but also their rehydrated counterparts were tested as well. It was determined that all HCs were thermally stable below 250 °C (Fig. S9.), therefore under reaction conditions shown as follows they are capable of keeping their chemical integrity.

A reaction time of 120 min in ethanol was applied at reflux temperature, using a 50 mg catalyst (Fig. S10.). Under these conditions, without catalyst benzaldehyde, conversion was not seen. On the other hand, all of the treated and commercial LDH-based samples exhibited measurable catalytic activity but with remarkable differences. The conversion of benzaldehyde over the different HCs decreased in the order of recon-M-HC > recon-S-HC > recon-C-HC > recon-HC > HC. During the optimization procedure, this order remained constant. For the most effective condensation, the catalyst loading of 100 mg was found to be optimal (Fig. S11.). Modified HCs proved to be robust catalysts for using them in any kind of solvents applied (Fig. S10.). Interestingly, polar protic solvents seemed to be more favorable to promote the condensation than any others. Their well-known water tolerance is of obvious importance, because condensation in the presence of water remains synthetic challenge with clear green chemical significance [88,89]. Strikingly, the onset temperatures of benzaldehyde conversion were found to decrease with the increasing specific surface area of the HCs. This may be connected to variations in the number of the accessible basic sites and/or their basic strengths influenced by the multistep treatment (Fig. S12.) [90]. The best catalytic performances were recorded at the same reaction temperature (50 °C) for all materials. Taking into consideration the total conversion of the reactants obtained under the optimized and very mild reaction conditions, it is noteworthy that all catalysts presented here were found to be competitive with any other benchmark catalysts. Because HTs have not exhibited results comparable with those of the corresponding HCs, we did not pay further attention to them (Fig. S13.).

The initial turnover frequency (TOF) values of the potential catalysts under the conditions presented above were determined from the linear part of the conversion versus time functions (Fig. 7A). In general, the pure and rehydrated HCs were less active catalysts, whereas each HC sample with ordered pore structure had significantly higher TOF values than the commercial ones. Among these, recon-M-HC was found to possess the highest TOF value (347.6 h^{-1}). In general, the appearance of porous fringes in HCs led to superior catalytic activities by more than 15 times relative to HC (Table 2). This implies a higher number of accessible basic sites on the surface of the porous HCs, resulting in significant variations in the reaction time to reach maximum conversions. With using recon-M-HC, total conversion was achieved within 25 min,

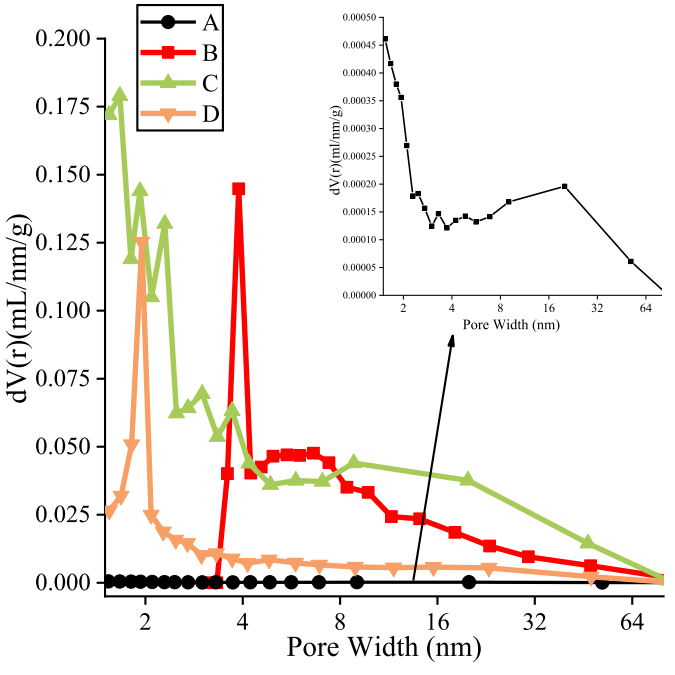

Fig. 6. Pore size distribution of HC (**A**); recon-M-HC (**B**); recon-S-HC (**C**); and recon-C-HC (**D**).

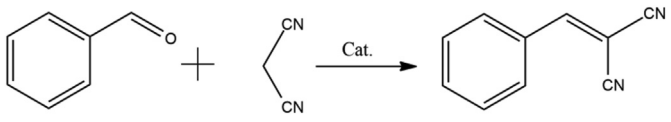

Scheme 2. Knoevenagel condensation between benzaldehyde and malononitrile.

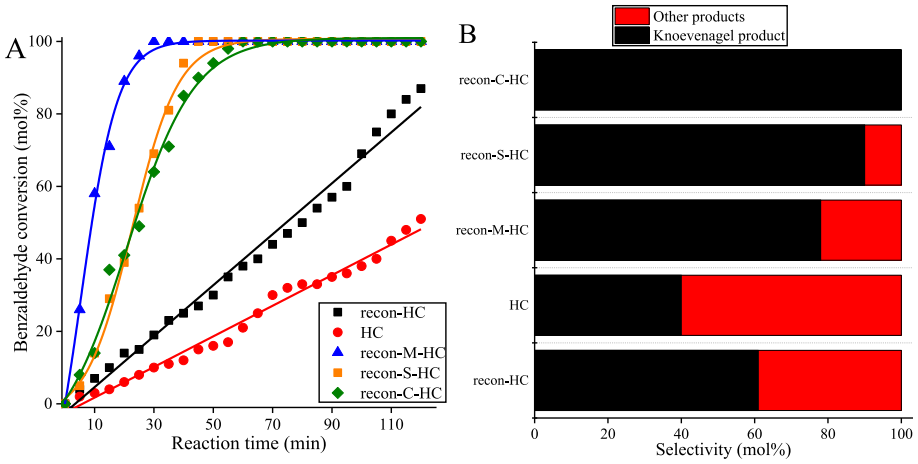

Fig. 7. Conversion data (**A**) and selectivities (**B**) of Knoevenagel condensation over the as-prepared and the variously modified HC samples between benzaldehyde (1.0 eq) and malononitrile (1.5 eq) using 0.1 g of catalyst and water (3 mL) as solvent, at 50 °C.

whereas after 120 min, only 50% benzaldehyde conversion was reached using HC (Table 2).

Selectivity toward benzylidenemalononitrile (Fig. 7B) over the HC samples increased in the order of HC < recon-HC < recon-M-HC < recon-S-HC < recon-C-HC under the optimized reaction conditions. This is clearly different from the order obtained for benzaldehyde conversion and points out that the differences in the catalytic performance may not only due solely to the increase in the number of available active sites but also depend on the nature of basic sites. Hence the characterization of the basic sites of the catalysts was undertaken.

To identify the possible variations in the Brønsted basicity of HCs, the samples were characterized by applying Hammett indicators (Fig. 8.) and CO_2-TPD measurements (Table S7.). From the data extracted from two independent methods practically, identical conclusions can be drawn; however, Hammett indicators enabled the direct investigation of the LDHs without using any heat treatment necessary for performing the desorption measurements. The abundance of the medium basic sites in the parent HCs was found to be negligible in comparison with the weak and strong ones. Interestingly, strong basic character could be associated with HCs, which is profoundly different from that of the HTs, as it was reported elsewhere [91]. A well-defined correlation can be seen between the basicity of HCs and their porosity and specific surface area. Accordingly, the ratio of the medium Brønsted basic sites and total concentration of the accessible basic sites increased with increase in the monoporous character. Furthermore, these markers changed inversely with the specific surface area; a trend opposite to this has been previously observed for surface-modified LDHs [92]. In addition, such a dramatic increase in the number of medium basic sites and extreme changes in the basic character have not been observed for treated LDHs reported. Taking into account all these factors, the generation of the considerable number of defect sites on the surface is likely to be the result of the post-synthetic treatment used in the present studies. These are most probably responsible for the remarkable changes in the basicity of the LDHs studied here [93]. Furthermore, these changes in the basicity of the LDHs can be associated with the differences in the actual molar ratio presented in Table 1. As hydroxyl groups coordinated to calcium centers have more contributions to the basicity of the HCs than others linked to aluminum centers [85]. Therefore, the actual molar ratio and its changes would be the key factor for the generation of more useful basic surfaces based on HCs.

The variations in the benzylidenemalononitrile selectivity achieved with various HC-based catalysts can be correlated with the basicity data shown above. By plotting the selectivity as a function of a number of medium basic sites, a linear function is obtained (Fig. 9A), indicating that the increase in the abundance of medium basic character facilitates the formation of the desired product, which is in line with the statement that the Knoevenagel condensation requires fine-tuned, moderately strong basic sites [27,93]. Besides, other types of condensation reactions may take place in the presence of stronger basic sites [23,27,93]. This may explain why the formation of undesired product(s) was observed. A Michael addition of malononitrile to benzylidenemalononitrile requiring very strong basic sites may take place. Most probably this is the reason why in the presence of recon-C-HC (with a low number of strong basic sites) by-product formation was not observed. Further control experiments with reduced amounts of malononitrile resulted in selectivities that were limited by the initial concentration of the nitrile, in line with our proposed

Table 2
The attributes of basic sites calculated from the titrations by Hammett indicators and initial turnover frequencies over the as-prepared and the modified CaAl-LDH samples.

Samples	Concentration of the basic sites (mmol/g)	Concentration of the weak basic sites (mmol/g)	Concentration of the medium basic sites (mmol/g)	Concentration of the strong basic sites (mmol/g)	Initial TOF (h^{-1})	Obtained yield% (after 30 minutes)
HC	0.45	0.05	0	0.40	7.9	10
recon-HC	0.55	0.11	0.09	0.35	29.9	19
recon-C-HC	0.75	0.18	0.4	0.17	136.7	64
recon-S-HC	0.78	0.23	0.32	0.23	136.9	69
recon-M-HC	0.90	0.30	0.25	0.35	347.6	100

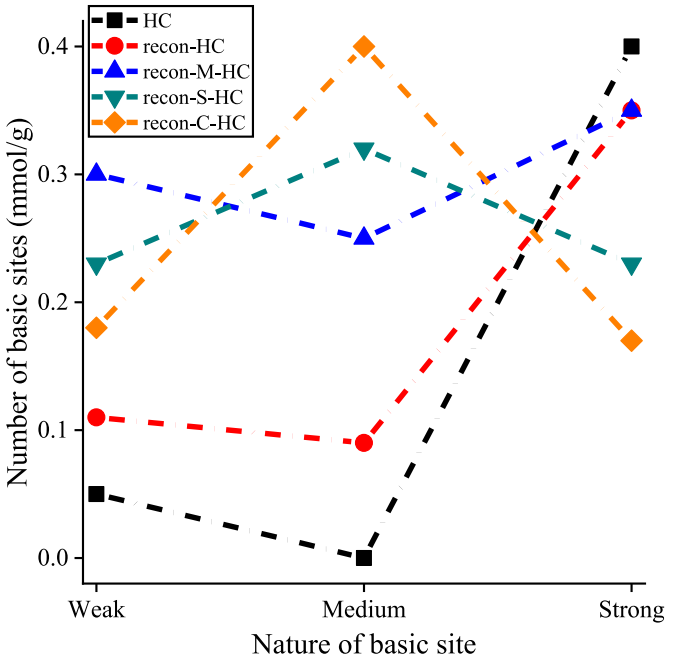

Fig. 8. Plot of the total number of basic sites for various HC samples. (Dash-dotted lines are just representative tools for better visualization.).

concept (Fig. S14.). Moreover, these facts indicated that, besides the condensation/addition, an additional process took place. By repeating the condensation with reduced nitrile concentration, however, under inert atmosphere, exclusive selectivity (with significantly reduced conversions) was detected, proving that the side reaction is the oxidation of benzaldehyde (Fig. S14).

Regarding TOF, no clear correlation with the nature of the accessible basic sites or porosity/specific surface area of the catalysts can be established (Fig. 9B). It seems that keeping all conditions constant, increasing the total concentration of the basic sites led to an increase of the TOF almost linearly from 7.9 to 136.9 h^{-1}. Owing to almost the same amount of accessible basic sites, recon-S-HC and recon-C-HC showed almost the same activity. Opposite to this, nevertheless, a larger TOF value was associated with recon-M-HC indicating a potential dependence of the activity on mesoporous-like structure/surface area too. Based on these findings, recon-M-HC provided the best activity, whereas recon-C-HC owned the highest selectivity among solid bases and zeolites under fairly mild conditions and without the need of using inert atmosphere (Table S1). Carbon-nitride- and ionic liquid-based catalysts proved to be more effective, however, with severe limitations in their recyclability (carbon-nitrides) and/or their handling to reach the optimal operation (ionic liquids).

To explore the stability and recyclability of surface-modified HCs, the heterogeneous samples were examined for five runs in the Knoevenagel condensation under the optimized reaction conditions (Fig. 10). First, it could be established that the activity of the parent samples (HC, recon-HC) considerably dropped in the second run, and this decrease continued until the stop of the catalytic reaction. By performing a Maitlis' test (hot filtration test) for the parent samples, partial homogeneous character of the condensation reaction could be observed, detecting significant benzylidenemalononitrile yield in the absence of the catalyst, too (Fig. S15.). With respect to leaching experiments followed by ICP-OES method, the filtered solution was found to contain a significant amount of calcium. Therefore, these catalysts are not stable and cannot be recycled. Their surface-modified counterparts, however, were reusable and heterogeneous in nature supported by hot filtration test and leaching experiments, respectively. The observed slight decrease in their activity during the second and third runs of the recycling experiments was owing to the absorption/adsorption of the reactants/products in the channels or on the surface of the HCs. This was further supported by the observation that recon-M-HC with the highest surface area was the least affected. In addition, based on the results of the XRD studies on the reused catalysts, it could be concluded that the well-known layered structure of the HCs remained intact after the third reaction cycle (Fig. S16.); however, their surface area was slightly altered (Fig. S17., Table S6.). Furthermore, control experiments also proved that the (colloidal) stability of the surface-modified HCs (recon-M-HC) was significantly enhanced relative to the parent sample, as justified by using time-resolved DLS method (Fig. S18.). The critical coagulation concentration (ccc) of the materials was determined by following the salt-induced aggregation of the LDH at different NaCl ionic strengths. The ccc value of HC was 6 mM, which is considered very low even amongst LDHs that show ccc values above 50 mM in the

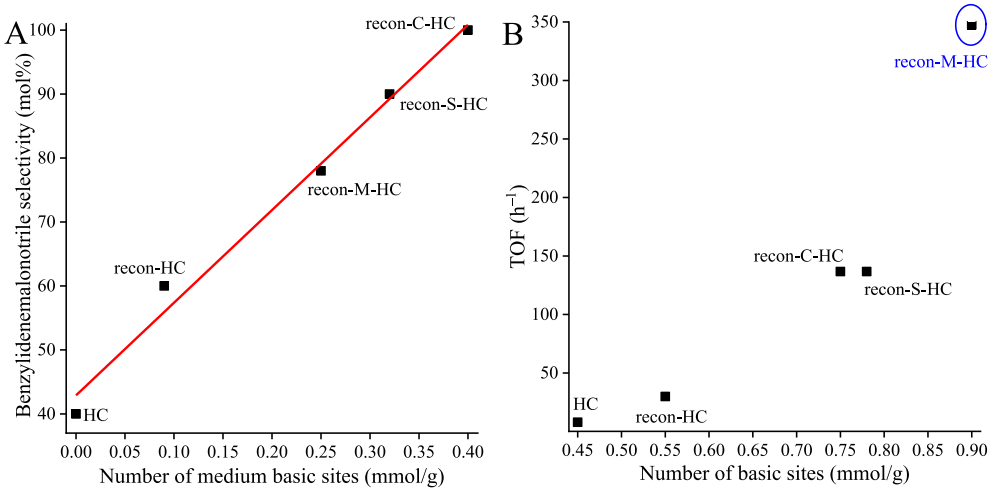

Fig. 9. Benzylidenemalonotrile selectivity data as a function of the number of medium basic sites (mmol/g) (**A**) and TOF (h^{-1}) values as a function of the total number of basic sites (mmol/g) (**B**) of Knoevenagel condensation over the as-prepared and the variously modified HC samples between benzaldehyde (1.0 eq) and malononitrile (1.5 eq) using 0.1 g of catalyst and water (3 mL) as solvents, at 50 °C for 25 min.

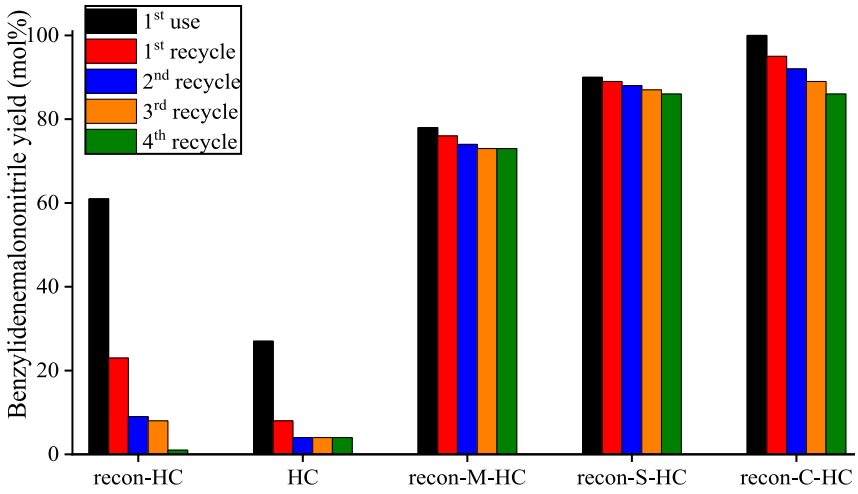

Fig. 10. Reusability data (benzylidenemalomomitrile yields) over the as-prepared as well as the modified HC catalysts in the Knoevenagel condensation between benzaldehyde (1.0 eq) and malononitrile (1.5 eq) using 0.1 g of catalyst, water (3 mL) as solvents, for 20 min (on using porous LDHs) or 80 min (on using non-porous counterparts) at 50 °C.

presence of NaCl ions [94]. On the other hand, the recon-M-HC did not reach fast aggregation below 1 M NaCl concentration; therefore, the sample possessed considerably higher colloidal stability than the HC.

The substrate scope of the condensation reaction was also investigated (Table 3). The robust HC-catalysis enabled the efficient condensations on aldehydes with *para* and *ortho* substitution arrangement. In all cases, activity and chemoselectivity were found to be really high under the optimized, mild reaction conditions. Strikingly, both electron-donating and electron-withdrawing functional groups were totally tolerated. More importantly, most of the markers (benzaldehyde conversion, benzylidenemalononitrile selectitvity) exhibited up to >95% value for both types of substituents. Furthermore, the designed catalysts showed excellent robustness for varying both the active methylene-containing compounds and aldehydes, respectively. As can be seen,on using active methylene group-containing compounds with less acidity, a slight decrease in the conversion was observed, albeit with constant selectivity. Significant variations in the order of the activity or selectivity of the HCs could not be observed regardless of the used reactants. The NMR data of the products can be found in the Supporting Information (Section 3.).

Considering all these findings, a reaction mechanism was created (Scheme S1.) on the basis of Corma et al.'s study [95]. In the proposed mechanism, the active methylene group of malononitrile was bound and deprotonated by the basic sites of the HCs, creating a stable surface conjugate. The generation of this anion gives rise to a nucleophilic attack onto the carbonyl carbon atom of benzaldehyde, producing the intermediate product followed by elimination of one water molecule and desorption of the product. It can be supposed, that when the stability of the intermediate product is too high — owing to the impact of the strong basic sites — the

Table 3
The scope of the reaction — conversion/TOF and selectivity results over the modified CaAl-LDH composite catalysts in the Knoevenagel condensation between benzaldehyde derivatives (1.0 eq) and active methylene group-containing compounds (1.5 eq) using 0.1 g of catalyst, at 50 °C for 30–60 min reaction time in aqueous solution.

samples	Aldehydes	Active methylene group-containing compound	Conversion (%)	Selectivity (%)	Reaction time (min)
recon-C-HC	2/4-chlorobenzaldehyde	Malononitrile	89/98	85/98	60
	2/4-nitrobenzaldehyde		94/95	91/97	60
	2/4-hydroxybenzaldehyde		81/90	80/89	60
	2/4-methylbenzaldehyde		87/91	82/81	60
	Butyraldehyde		90	88	60
	Benzaldehyde		100	100	60
	Benzaldehyde	Ethylcyanoacetate	87	95	60
		Diethylmalonate	80	97	60
recon-S-HC	2/4-chlorobenzaldehyde	Malononitrile	94/100	90/92	30
	2/4-nitrobenzaldehyde		93/100	94/93	30
	2/4-hydroxybenzaldehyde		79//87	85/91	60
	2/4-methylbenzaldehyde		85/84	88/86	60
	Butyraldehyde		91	91	60
	Benzaldehyde		100	90	45
	Benzaldehyde	Ethylcyanoacetate	92	92	60
		Diethylmalonate	86	89	60
recon-M-HC	2/4-chlorobenzaldehyde	Malononitrile	97/99	82/80	25
	2/4-nitrobenzaldehyde		94/94	84/77	25
	2/4-hydroxybenzaldehyde		74/80	85/71	30
	2/4-methylbenzaldehyde		80/81	74/75	30
	Butyraldehyde		94	77	45
	Benzaldehyde		100	78	30
	Benzaldehyde	Ethylcyanoacetate	98	80	45
		Diethylmalonate	91	82	45

possibility for carrying out above-mentioned side reaction strongly increases.

4. Conclusions

In conclusion, three efficient, well-designed synthesis strategies were developed to prepare surface-engineered LDHs. Especially, HCs and HTs with regulated pore structure were prepared using sacrificial templates (MWCNT, CTAB, and SBA-15), and a useful water-based sol-gel synthesis method was elaborated without the need of using a hyperalkaline medium. A simple post-synthetic treatment with heating or acidic handling followed by the reconstruction method was developed resulting in template-free porous LDHs. A clear relationship between the morphology of the template-loaded, parent composites, and the pore structure of the final products was established. The obtained structures have high surface area, unique pore structure, and remarkably enhanced total pore volume. Accordingly, by considering the morphological aspects, the construction and implementation of unique microporous and mesoporous-like nanostructured LDHs as well as brucite-like structures with mixed pore structure were successful. Furthermore, the applied dosage and the removal of the templates not only facilitated the synthesis of porous LDH but also contributed to the changes in the abundance of the various (weak, medium, and strong) basic sites of HCs, as supported by Hammett investigations. These are most probably associated with the formation of defect sites on the surface during these treatments.

In addition, it was also found that the catalytic activity, selectivity, and robustness of the HC/HT-based catalysts in a Knovenagel condensation largely depend on the porosity or number of accessible basic sites as well as with the strength of them. In the presence of porous LDHs, condensation occurred in high yields and exclusive selectivity with a wide functional group tolerance under ambient reaction conditions in water in a really useful timescale. While the product selectivity was strongly improved with increasing the number of accessible medium basic sites, a high reaction rate could be achieved by nanostructured LDH with mesoporous-like structure. Moreover, because of their high colloid stability, porous catalysts proved to be reusable catalysts as opposed to the parent samples that behaved as homogeneous catalysts. Thus, it could be concluded that all relevant factors concerning effective condensations depend on the modified-surface area and thus indirectly on the morphology of the parent composites. Our results can be useful to design and develop effective solid bases with modified porosity and surface area for potential catalytic applications.

CRediT author statement

Sz. Muráth: Investigation, Methodology, Data curation, Writing – original draft. **T. Varga:** Investigation, Data curation. **Á. Kukovecz:** Resources, Data curation.**Z. Kónya:** Resources, Data curation. **P. Sipos:** Funding acquisition, Resources, Writing – original draft. **I. Pálinkó:** Funding acquisition, Resources. **G. Varga:** Conceptualization, Supervision, Investigation, Methodology, Data curation, Writing – original draft, Writing – review & editing.

Declaration of competing interest

The authors declare that they have no known competing financial interests or personal relationships that could have appeared to influence the work reported in this article.

Acknowledgments

This work was supported by the Hungarian Government and the European Union through grant GINOP-2.3.2-15-2016-00013. The financial support is highly appreciated. One of us, G. Varga thanks for the postdoctoral fellowship under the grant PD 128189, and he also appreciates the support of NTP-NFTÖ-20-B program. This workwas also supported by University of Szeged Open Access Fund (Grant number:5564).

Appendix A. Supplementary data

Supplementary data to this article can be found online at https://doi.org/10.1016/j.mtchem.2021.100682.

References

[1] X. Gu, Y. Tang, X. Zhang, Z. Luo, H. Lu, Organocatalytic Knoevenagel condensation by chiral: C2-symmetric tertiary diamines, New J. Chem. 40 (2016) 6580–6583, https://doi.org/10.1039/c6nj00613b.
[2] N. Mase, T. Horibe, Organocatalytic knoevenagel condensations by means of carbamic acid ammonium salts, Org. Lett. 15 (2013) 1854–1857, https://doi.org/10.1021/ol400462d.
[3] X. Liu, X. Li, Z. Wang, J. Zhou, X. Fan, Y. Fu, Biosynthesis of α-substituted β-Ketoesters via the tandem knoevenagel condensation-reduction reaction using a single enzyme, ACS Sustain. Chem. Eng. 8 (2020) 8206–8213, https://doi.org/10.1021/acssuschemeng.0c00938.
[4] V. Arredondo, D.E. Roa, S. Yan, F. Liu-Smith, D.L. Van Vranken, Total synthesis of (±)-Pestalachloride C and (±)-Pestalachloride D through a biomimetic knoevenagel/hetero-diels-alder cascade, Org. Lett. 21 (2019) 1755–1759, https://doi.org/10.1021/acs.orglett.9b00323.
[5] A. Corma, R.M. Martín-Aranda, Application of solid base catalysts in the preparation of prepolymers by condensation of ketones and malononitrile, Appl. Catal. Gen. 105 (1993) 271–279, https://doi.org/10.1016/0926-860X(93)80252-L.
[6] F. Liang, Y.J. Pu, T. Kurata, J. Kido, H. Nishide, Synthesis and electroluminescent property of poly(p-phenylenevinylene)s bearing triarylamine pendants, Polymer (Guildf) 46 (2005) 3767–3775, https://doi.org/10.1016/j.polymer.2005.03.036.
[7] P. Knochel, G.A. Molander, Comprehensive Organic Synthesis, second ed., Elsevier, 2014.
[8] R.A. Sheldon, H. Van Bekkum, Fine Chemicals through Heterogeneous Catalysis, John Wiley & Sons, Weinheim, 2008.
[9] J.J. Shrikhande, M.B. Gawande, R.V. Jayaram, Cross-aldol and Knoevenagel condensation reactions in aqueous micellar media, Catal. Commun. 9 (2008) 1010–1016, https://doi.org/10.1016/j.catcom.2007.10.001.
[10] B. Sarmah, B. Satpati, R. Srivastava, Highly efficient and recyclable basic mesoporous zeolite catalyzed condensation, hydroxylation, and cycloaddition reactions, J. Colloid Interface Sci. 493 (2017) 307–316, https://doi.org/10.1016/j.jcis.2017.01.039.
[11] A. Corma, From microporous to mesoporous molecular sieve materials and their use in catalysis, Chem. Rev. 97 (1997) 2373–2419, https://doi.org/10.1021/cr960406n.
[12] T.F. Chaves, H.O. Pastore, P. Hammer, D. Cardoso, As-synthesized TEA-BEA zeolite: effect of Si/Al ratio on the Knoevenagel condensation, Microporous Mesoporous Mater. 202 (2015) 198–207, https://doi.org/10.1016/j.micromeso.2014.09.058.
[13] A. Wojtaszek-Gurdak, V. Calvino-Casilda, A. Grzesinska, R. Martin-Aranda, M. Ziolek, Impact of Brønsted acid sites in MWW zeolites modified with cesium and amine species on Knoevenagel condensation, Microporous Mesoporous Mater. 280 (2019) 288–296, https://doi.org/10.1016/j.micromeso.2019.02.007.
[14] A. Kawano, T. Moteki, M. Ogura, Effect of delamination on active base site formation over nitrided MWW-type zeolite for Knoevenagel condensation, Microporous Mesoporous Mater. 299 (2020) 110104, https://doi.org/10.1016/j.micromeso.2020.110104.
[15] N.P. Tangale, S.K. Sonar, P.S. Niphadkar, P.N. Joshi, Hierarchical K/LTL zeolites: synthesis by alkali treatment, characterization and catalytic performance in Knoevenagel condensation reaction, J. Ind. Eng. Chem. 40 (2016) 128–136, https://doi.org/10.1016/j.jiec.2016.06.016.
[16] Y.V.S. Rao, D.E. De Vos, P.A. Jacobs, 1,5,7-Triazabicyclo[4.4.0]dec-5-ene immobilized in MCM-41: a strongly basic porous catalyst, Angew Chem. Int. Ed. Engl. 36 (1997) 2661–2663, https://doi.org/10.1002/anie.199726611.
[17] J.N. Appaturi, M. Selvaraj, S.B. Abdul Hamid, M.R. Bin Johan, Synthesis of 3-(2-furylmethylene)-2,4-pentanedione using DL-Alanine functionalized MCM-41 catalyst via Knoevenagel condensation reaction, Microporous Mesoporous Mater. 260 (2018) 260–269, https://doi.org/10.1016/j.micromeso.2017.03.031.
[18] J.N. Appaturi, T. Pulingam, J.R. Rajabathar, F. Khoerunnisa, T.C. Ling, S.H. Tan, E.P. Ng, Acid-base bifunctional SBA-15 as an active and selective catalyst for synthesis of ethyl α-cyanocinnamate via Knoevenagel condensation,

Microporous Mesoporous Mater. 320 (2021) 111091, https://doi.org/10.1016/j.micromeso.2021.111091.
[19] Y. Kuwahara, K. Tsuji, T. Ohmichi, T. Kamegawa, K. Mori, H. Yamashita, Waste-slag hydrocalumite and derivatives as heterogeneous base catalysts, ChemSusChem 5 (2012) 1523–1532, https://doi.org/10.1002/cssc.201100814.
[20] K. Ebitani, K. Motokura, K. Mori, T. Mizugaki, K. Kaneda, Reconstructed hydrotalcite as a highly active heterogeneous base catalyst for carbon-carbon bond formations in the presence of water, J. Org. Chem. 71 (2006) 5440–5447, https://doi.org/10.1021/jo060345l.
[21] T. Li, W. Zhang, W. Chen, H.N. Miras, Y.F. Song, Layered double hydroxide anchored ionic liquids as amphiphilic heterogeneous catalysts for the Knoevenagel condensation reaction, Dalton Trans. 47 (2018) 3059–3067, https://doi.org/10.1039/c7dt03665e.
[22] G. Varga, M. Szabados, Á. Kukovecz, Z. Kónya, T. Varga, P. Sipos, I. Pálinkó, Layered double alkoxides a novel group of layered double hydroxides without water content, Mater. Res. Lett. 8 (2020) 68–74, https://doi.org/10.1080/21663831.2019.1700199.
[23] T. Jose, J. Ftouni, P.C.A. Bruijnincx, Structured hydroxyapatite composites as efficient solid base catalysts for condensation reactions, Catal. Sci. Technol. 11 (2021) 3428–3436, https://doi.org/10.1039/d1cy00102g.
[24] J.P.H. Li, A.A. Adesina, E.M. Kennedy, M. Stockenhuber, A mechanistic study of the Knoevenagel condensation reaction: new insights into the influence of acid and base properties of mixed metal oxide catalysts on the catalytic activity, Phys. Chem. Chem. Phys. 19 (2017) 26630–26644, https://doi.org/10.1039/c7cp04743f.
[25] X. Yuan, Z. Wang, Q. Zhang, J. Luo, An intramolecular relay catalysis strategy for Knoevenagel condensation and 1,3-dipolar cycloaddition domino reactions, RSC Adv. 9 (2019) 23614–23621, https://doi.org/10.1039/c9ra04081a.
[26] Q. Xu, Y. Niu, G. Wang, Y. Li, Y. Zhao, V. Singh, J. Niu, J. Wang, Polyoxoniobates as a superior Lewis base efficiently catalyzed Knoevenagel condensation, Mol. Catal. 453 (2018) 93–99, https://doi.org/10.1016/j.mcat.2018.05.002.
[27] A. Corma, V. Fornés, R.M. Martín-Aranda, F. Rey, Determination of base properties of hydrotalcites: condensation of benzaldehyde with ethyl acetoacetate, J. Catal. 134 (1992) 58–65, https://doi.org/10.1016/0021-9517(92)90209-Z.
[28] M.J. Climent, A. Corma, V. Fornés, A. Frau, R. Guil-López, S. Iborra, J. Primo, Aluminophosphates oxynitrides as base catalysts: nature of the base sites and their catalytic implications, J. Catal. 163 (1996) 392–398, https://doi.org/10.1006/jcat.1996.0340.
[29] J.P.H. Li, E.M. Kennedy, A.A. Adesina, M. Stockenhuber, Mechanistic insights into the Knoevenagel condensation reaction over ZnO catalysts: direct observation of surface intermediates using in situ FTIR, J. Catal. 369 (2019) 157–167, https://doi.org/10.1016/j.jcat.2018.10.039.
[30] J.N. Appaturi, R. Ratti, B.L. Phoon, S.M. Batagarawa, I.U. Din, M. Selvaraj, R.J. Ramalingam, A review of the recent progress on heterogeneous catalysts for Knoevenagel condensation, Dalton Trans. 50 (2021) 4445–4469, https://doi.org/10.1039/d1dt00456e.
[31] B. Sarmah, R. Srivastava, P. Manjunathan, G.V. Shanbhag, Green and sustainable tandem catalytic approach for fine-chemicals synthesis using octahedral MnO2 molecular sieve: catalytic activity versus method of catalyst synthesis, ACS Sustain. Chem. Eng. 3 (2015) 2933–2943, https://doi.org/10.1021/acssuschemeng.5b00896.
[32] X. Li, B. Lin, H. Li, Q. Yu, Y. Ge, X. Jin, X. Liu, Y. Zhou, J. Xiao, Carbon doped hexagonal BN as a highly efficient metal-free base catalyst for Knoevenagel condensation reaction, Appl. Catal. B Environ. 239 (2018) 254–259, https://doi.org/10.1016/j.apcatb.2018.08.021.
[33] H. An, J. Zhang, S. Chang, Y. Hou, Q. Zhu, 2D hybrid architectures constructed from two kinds of polyoxovanadates as efficient heterogeneous catalysts for cyanosilylation and knoevenagel condensation, Inorg. Chem. 59 (2020) 10578–10590, https://doi.org/10.1021/acs.inorgchem.0c00999.
[34] M. Tavakolian, M.M. Najafpour, Molybdenum carbide as an efficient and durable catalyst for aqueous Knoevenagel condensation, New J. Chem. 43 (2019) 16437–16440, https://doi.org/10.1039/C9NJ04647J.
[35] B. Şen, E.H. Akdere, A. Şavk, E. Gültekin, Ö. Paralı, H. Göksu, F. Şen, A novel thiocarbamide functionalized graphene oxide supported bimetallic monodisperse Rh-Pt nanoparticles (RhPt/TC@GO NPs) for Knoevenagel condensation of aryl aldehydes together with malononitrile, Appl. Catal. B Environ. 225 (2018) 148–153, https://doi.org/10.1016/j.apcatb.2017.11.067.
[36] Z. Alirezvani, M.G. Dekamin, E. Valiey, Cu(II) and magnetite nanoparticles decorated melamine-functionalized chitosan: a synergistic multifunctional catalyst for sustainable cascade oxidation of benzyl alcohols/Knoevenagel condensation, Sci. Rep. 9 (2019) 1–12, https://doi.org/10.1038/s41598-019-53765-3.
[37] R. Srirambalaji, S. Hong, R. Natarajan, M. Yoon, R. Hota, Y. Kim, Y.H. Ko, K. Kim, Tandem catalysis with a bifunctional site-isolated Lewis acid–Brønsted base metal–organic framework, NH2-MIL-101(Al), Chem. Commun. 48 (2012) 11650–11652, https://doi.org/10.1039/c2cc36678a.
[38] M.L. Gao, M.H. Qi, L. Liu, Z.B. Han, An exceptionally stable core-shell MOF/COF bifunctional catalyst for a highly efficient cascade deacetalization-Knoevenagel condensation reaction, Chem. Commun. 55 (2019) 6377–6380, https://doi.org/10.1039/c9cc02174d.
[39] K. Cai, W. Tan, N. Zhao, H. He, Design and assembly of a hierarchically micro- and mesoporous MOF as a highly efficient heterogeneous catalyst for knoevenagel condensation reaction, Cryst. Growth Des. 20 (2020) 4845–4851, https://doi.org/10.1021/acs.cgd.0c00636.
[40] C. Guo, Y. Zhang, L. Zhang, Y. Zhang, J. Wang, 2-Methylimidazole-assisted synthesis of a two-dimensional MOF-5 catalyst with enhanced catalytic activity for the Knoevenagel condensation reaction, CrystEngComm 20 (2018) 5327–5331, https://doi.org/10.1039/c8ce00954f.
[41] A. Bahuguna, A. Kumar, T. Chhabra, A. Kumar, V. Krishnan, Potassium-Functionalized graphitic carbon nitride supported on reduced graphene oxide as a sustainable catalyst for knoevenagel condensation, ACS Appl. Nano Mater. 1 (2018) 6711–6723, https://doi.org/10.1021/acsanm.8b01524.
[42] A. Rashidizadeh, H.R. Esmaili Zand, H. Ghafuri, Z. Rezazadeh, Graphitic carbon nitride nanosheet/FeWO4Nanoparticle composite for tandem photooxidation/knoevenagel condensation, ACS Appl. Nano Mater. 3 (2020) 7057–7065, https://doi.org/10.1021/acsanm.0c01380.
[43] N.D. Shcherban, P. Mäki-Arvela, A. Aho, S.A. Sergiienko, P.S. Yaremov, K. Eränen, D.Y. Murzin, Melamine-derived graphitic carbon nitride as a new effective metal-free catalyst for Knoevenagel condensation of benzaldehyde with ethylcyanoacetate, Catal. Sci. Technol. 8 (2018) 2928–2937, https://doi.org/10.1039/c8cy00253c.
[44] D. Meng, Y. Qiao, X. Wang, W. Wen, S. Zhao, DABCO-catalyzed Knoevenagel condensation of aldehydes with ethyl cyanoacetate using hydroxy ionic liquid as a promoter, RSC Adv. 8 (2018) 30180–30185, https://doi.org/10.1039/c8ra06506c.
[45] L.C. Player, B. Chan, P. Turner, A.F. Masters, T. Maschmeyer, Bromozincate ionic liquids in the Knoevenagel condensation reaction, Appl. Catal. B Environ. 223 (2018) 228–233, https://doi.org/10.1016/j.apcatb.2017.09.021.
[46] H. Xu, L. Pan, X. Fang, B. Liu, W. Zhang, M. Lu, Y. Xu, T. Ding, H. Chang, Knoevenagel condensation catalyzed by novel Nmm-based ionic liquids in water, Tetrahedron Lett. 58 (2017) 2360–2365, https://doi.org/10.1016/j.tetlet.2017.05.006.
[47] B.M. Choudary, M. Lakshmi Kantam, V. Neeraja, K. Koteswara Rao, F. Figueras, L. Delmotte, Layered double hydroxide fluoride: a novel solid base catalyst for C-C bond formation, Green Chem. 3 (2001) 257–260, https://doi.org/10.1039/b107124f.
[48] U. Costantino, M. Curini, F. Montanari, M. Nocchetti, O. Rosati, Hydrotalcite-like compounds as catalysts in liquid phase organic synthesis I. Knoevenagel condensation promoted by $[Ni_{0.73}Al_{0.27}(OH)_2](CO_3)_{0.135}$, J. Mol. Catal. A Chem. 195 (2003) 245–252, https://doi.org/10.1016/S1381-1169(02)00580-0.
[49] V. Prevot, Y. Tokudome, 3D hierarchical and porous layered double hydroxide structures: an overview of synthesis methods and applications, J. Mater. Sci. 52 (2017) 11229–11250, https://doi.org/10.1007/s10853-017-1067-9.
[50] C. Zhang, M. Shao, L. Zhou, Z. Li, K. Xiao, M. Wei, Hierarchical NiFe layered double hydroxide hollow microspheres with highly-efficient behavior toward oxygen evolution reaction, ACS Appl. Mater. Interfaces 8 (2016) 33697–33703, https://doi.org/10.1021/acsami.6b12100.
[51] L. Li, R. Ma, N. Iyi, Y. Ebina, K. Takada, T. Sasaki, Hollow nanoshell of layered double hydroxide, Chem. Commun. 2 (2006) 3125–3127, https://doi.org/10.1039/b605889b.
[52] J. Li, N. Zhang, D.H.L. Ng, Synthesis of a 3D hierarchical structure of γ-AlO(OH)/Mg-Al-LDH/C and its performance in organic dyes and antibiotics adsorption, J. Mater. Chem. A. 3 (2015) 21106–21115, https://doi.org/10.1039/c5ta04497a.
[53] J.J. Woodford, J.P. Dacquin, K. Wilson, A.F. Lee, Better by design: nano-engineered macroporous hydrotalcites for enhanced catalytic biodiesel production, Energy Environ. Sci. 5 (2012) 6145–6150, https://doi.org/10.1039/c2ee02837a.
[54] S.S.L. Sobhana, D.R. Bogati, M. Reza, J. Gustafsson, P. Fardim, Cellulose biotemplates for layered double hydroxides networks, Microporous Mesoporous Mater. 225 (2016) 66–73, https://doi.org/10.1016/j.micromeso.2015.12.009.
[55] Z. Gu, J.J. Atherton, Z.P. Xu, Hierarchical layered double hydroxide nanocomposites: structure, synthesis and applications, Chem. Commun. 51 (2015) 3024–3036, https://doi.org/10.1039/c4cc07715f.
[56] H. Wang, X. Xiang, F. Li, Facile synthesis and novel electrocatalytic performance of nanostructured Ni-Al layered double hydroxide/carbon nanotube composites, J. Mater. Chem. 20 (2010) 3944–3952, https://doi.org/10.1039/b924911g.
[57] H. Suo, H. Duan, C. Chen, J.C. Buffet, D. O'Hare, Bifunctional acid-base mesoporous silica@aqueous miscible organic-layered double hydroxides, RSC Adv. 9 (2019) 3749–3754, https://doi.org/10.1039/c9ra00188c.
[58] D. O'Hare, M. Lyu, C. Chen, J.C. Buffet, A facile synthesis of layered double hydroxide based core@shell hybrid materials, New J. Chem. 44 (2020) 10095–10101, https://doi.org/10.1039/c9nj06341b.
[59] J. Liu, R. Harrison, J.Z. Zhou, T.T. Liu, C. Yu, G.Q. Lu, S.Z. Qiao, Z.P. Xu, Synthesis of nanorattles with layered double hydroxide core and mesoporous silica shell as delivery vehicles, J. Mater. Chem. 21 (2011) 10641–10644, https://doi.org/10.1039/c1jm12054a.
[60] H. Chen, L. Hu, M. Chen, Y. Yan, L. Wu, Nickel-cobalt layered double hydroxide nanosheets for high-performance supercapacitor electrode materials, Adv. Funct. Mater. 24 (2014) 934–942, https://doi.org/10.1002/adfm.201301747.
[61] L. Sun, C. Hu, Facile synthesis via a solvothermal route and characterization of Mg-Al layered double hydroxide (LDH) 3D micro-nano structures, Mater. Res. Bull. 46 (2011) 1922–1927, https://doi.org/10.1016/j.materresbull.2011.07.022.
[62] Y. Kuwahara, K. Tsuji, T. Ohmichi, T. Kamegawa, K. Mori, H. Yamashita, Transesterifications using a hydrocalumite synthesized from waste slag: an economical and ecological route for biofuel production, Catal. Sci. Technol. 2 (2012) 1842–1851, https://doi.org/10.1039/c2cy20113e.

[63] M. Szabados, A. Adél Ádám, P. Traj, S. Muráth, K. Baán, P. Bélteky, Z. Kónya, Á. Kukovecz, P. Sipos, I. Pálinkó, Mechanochemical and wet chemical syntheses of CaIn-layered double hydroxide and its performance in a transesterification reaction compared to those of other Ca2M(III) hydrocalumites (M: Al, Sc, V, Cr, Fe, Ga) and Mg(II)-, Ni(II)-, Co(II)- or Zn(II)-based, J. Catal. 391 (2020) 282–297, https://doi.org/10.1016/j.jcat.2020.07.038.
[64] S. Muráth, Z. Somosi, Á. Kukovecz, Z. Kónya, P. Sipos, I. Pálinkó, Novel route to synthesize CaAl- and MgAl-layered double hydroxides with highly regular morphology, J. Sol. Gel Sci. Technol. 89 (2019) 844–851, https://doi.org/10.1007/s10971-018-4903-8.
[65] X.Y. Jin, K.J. Kim, H.S. Lee, Grazing incidence reflection absorption Fourier transform infrared (GIRA-FTIR) spectroscopic studies on the ferroelectric behavior of poly(vinylidene fluoride-trifluoroethylene) ultrathin films, Polymer (Guildf) 46 (2005) 12410–12415, https://doi.org/10.1016/j.polymer.2005.10.066.
[66] A. Navajas, I. Campo, G. Arzamendi, W.Y. Hernández, L.F. Bobadilla, M.A. Centeno, J.A. Odriozola, L.M. Gandía, Synthesis of biodiesel from the methanolysis of sunflower oil using PURAL® Mg-Al hydrotalcites as catalyst precursors, Appl. Catal. B Environ. 100 (2010) 299–309, https://doi.org/10.1016/j.apcatb.2010.08.006.
[67] Y. Chen, X. Wang, Y. Bao, W. Wu, Study on structure and fluorescence of Tb-doped CaAl LDHs prepared in ethanol/water system, J. Sol. Gel Sci. Technol. 81 (2017) 413–422, https://doi.org/10.1007/s10971-016-4216-8.
[68] G.Y. Abo El-Reesh, A.A. Farghali, M. Taha, R.K. Mahmoud, Novel synthesis of Ni/Fe layered double hydroxides using urea and glycerol and their enhanced adsorption behavior for Cr(VI) removal, Sci. Rep. 10 (2020) 1–20, https://doi.org/10.1038/s41598-020-57519-4.
[69] G. Varga, Á. Kukovecz, Z. Kónya, L. Korecz, S. Muráth, Z. Csendes, G. Peintler, S. Carlson, P. Sipos, I. Pálinkó, Mn(II)-amino acid complexes intercalated in CaAl-layered double hydroxide - well-characterized, highly efficient, recyclable oxidation catalysts, J. Catal. 335 (2016) 125–134, https://doi.org/10.1016/j.jcat.2015.12.023.
[70] M. Pavlovic, P. Rouster, E. Bourgeat-Lami, V. Prevot, I. Szilagyi, Design of latex-layered double hydroxide composites by tuning the aggregation in suspensions, Soft Matter 13 (2017) 842–851, https://doi.org/10.1039/c6sm02608g.
[71] S. Kumar, R. Walia, A. Kumar, V. Verma, Hybrid structure of MWCNT/ferrite and GO incorporated composites for microwave shielding properties and their practical applications, RSC Adv. 11 (2021) 9775–9787, https://doi.org/10.1039/d1ra01129d.
[72] G. Varga, S. Ziegenheim, S. Muráth, Z. Csendes, Á. Kukovecz, Z. Kónya, S. Carlson, L. Korecz, E. Varga, P. Pusztai, P. Sipos, I. Pálinkó, Cu(II)-amino acid–CaAl-layered double hydroxide complexes, recyclable, efficient catalysts in various oxidative transformations, J. Mol. Catal. A Chem. 423 (2016) 49–60, https://doi.org/10.1016/j.molcata.2016.06.008.
[73] Y. Zhao, F. Li, R. Zhang, D.G. Evans, X. Duan, Preparation of layered double-hydroxide nanomaterials with a uniform crystallite size using a new method involving separate nucleation and aging steps, Chem. Mater. 14 (2002) 4286–4291, https://doi.org/10.1021/cm020370h.
[74] J.T. Kloprogge, D. Wharton, L. Hickey, R.L. Frost, Infrared and Raman study of interlayer carbonate anions in Mg/Al hydrotalcite, Am. Mineral. 87 (2002) 623–629.
[75] M. Domínguez, M.E. Pérez-Bernal, R.J. Ruano-Casero, C. Barriga, V. Rives, R.A.S. Ferreira, L.D. Carlos, J. Rocha, Multiwavelength luminescence in lanthanide-doped hydrocalumite and mayenite, Chem. Mater. 23 (2011) 1993–2004, https://doi.org/10.1021/cm200408x.
[76] G. Varga, Z. Somosi, Z. Kónya, Á. Kukovecz, I. Pálinkó, I. Szilagyi, A colloid chemistry route for the preparation of hierarchically ordered mesoporous layered double hydroxides using surfactants as sacrificial templates, J. Colloid Interface Sci. 581 (2021) 928–938, https://doi.org/10.1016/j.jcis.2020.08.118.
[77] Y. Gao, G. Chen, X. Wang, H. Yang, Z. Wang, W. Lin, H. Xu, Y. Bai, C. Wu, PY13FSI-infiltrated SBA-15 as nonflammable and high ion-conductive ionogel electrolytes for quasi-solid-state sodium-ion batteries, ACS Appl. Mater. Interfaces 12 (2020) 22981–22991, https://doi.org/10.1021/acsami.0c04878.
[78] M. Sun, P. Zhang, D. Wu, R.L. Frost, Novel approach to fabricate organo-LDH hybrid by the intercalation of sodium hexadecyl sulfate into tricalcium aluminate, Appl. Clay Sci. 140 (2017) 25–30, https://doi.org/10.1016/j.clay.2017.01.026.
[79] M. Pavlovic, P. Rouster, T. Oncsik, I. Szilagyi, Tuning colloidal stability of layered double hydroxides: from monovalent ions to polyelectrolytes, Chempluschem 82 (2017) 121–131, https://doi.org/10.1002/cplu.201600295.
[80] B. Xiao, W.H. Zhang, H.F. Xia, Z.T. Wang, L.B. Tang, C.S. An, Z.J. He, H. Tong, J.C. Zheng, $V_2(PO_4)O$/C@CNT hollow spheres with a core-shell structure as a high performance anode material for lithium-ion batteries, Mater. Chem. Front. 3 (2019) 456–463, https://doi.org/10.1039/c8qm00619a.
[81] R. Li, Z. Hu, X. Shao, P. Cheng, S. Li, W. Yu, W. Lin, D. Yuan, Large scale synthesis of NiCo layered double hydroxides for superior asymmetric electrochemical capacitor, Sci. Rep. 6 (2016) 1–9, https://doi.org/10.1038/srep18737.
[82] W.L.J. Kwok, H. Suo, C. Chen, D.W.J. Leung, J.C. Buffet, D. O'Hare, Synthesis of dense porous layered double hydroxides from struvite, Green Chem. 23 (2021) 1616–1620, https://doi.org/10.1039/d0gc04410e.
[83] L. Mohapatra, K.M. Parida, Dramatic activities of vanadate intercalated bismuth doped LDH for solar light photocatalysis, Phys. Chem. Chem. Phys. 16 (2014) 16985–16996, https://doi.org/10.1039/c4cp01665c.
[84] Y. Zhao, G. Chen, T. Bian, C. Zhou, G.I.N. Waterhouse, L.Z. Wu, C.H. Tung, L.J. Smith, D. O'Hare, T. Zhang, Defect-rich ultrathin ZnAl-layered double hydroxide nanosheets for efficient photoreduction of CO2 to CO with water, Adv. Mater. 27 (2015) 7824–7831, https://doi.org/10.1002/adma.201503730.
[85] W. Bing, L. Zheng, S. He, D. Rao, M. Xu, L. Zheng, B. Wang, Y. Wang, M. Wei, Insights on active sites of CaAl-hydrotalcite as a high-performance solid base catalyst toward aldol condensation, ACS Catal. 8 (2018) 656–664, https://doi.org/10.1021/acscatal.7b03022.
[86] C. Chen, M. Yang, Q. Wang, J.C. Buffet, D. O'Hare, Synthesis and characterisation of aqueous miscible organic-layered double hydroxides, J. Mater. Chem. A. 2 (2014) 15102–15110, https://doi.org/10.1039/c4ta02277g.
[87] P. Gunawan, R. Xu, Direct assembly of anisotropic layered double hydroxide (LDH) nanocrystals on spherical template for fabrication of drug-LDH hollow nanospheres, Chem. Mater. 21 (2009) 781–783, https://doi.org/10.1021/cm803203x.
[88] Z.S. Zhao, Y. Zhang, T. Fang, Z.B. Han, F.S. Liang, Chitosan-coated metal-organic-framework nanoparticles as catalysts for tandem deacetalization-knoevenagel condensation reactions, ACS Appl. Nano Mater. 3 (2020) 6316–6320, https://doi.org/10.1021/acsanm.0c01486.
[89] D. Patel, R. Vithalani, C.K. Modi, Highly efficient FeNP-embedded hybrid bifunctional reduced graphene oxide for Knoevenagel condensation with active methylene compounds, New J. Chem. 44 (2020) 2868–2881, https://doi.org/10.1039/c9nj05821d.
[90] W. Tang, Y. Deng, W. Li, J. Li, G. Liu, S. Li, X. Wu, Y. Chen, Importance of porous structure and synergistic effect on the catalytic oxidation activities over hierarchical Mn-Ni composite oxides, Catal. Sci. Technol. 6 (2016) 1710–1718, https://doi.org/10.1039/c5cy01119a.
[91] D.W.J. Leung, C. Chen, J.C. Buffet, D. O'Hare, Correlations of acidity-basicity of solvent treated layered double hydroxides/oxides and their CO_2 capture performance, Dalton Trans. 49 (2020) 9306–9311, https://doi.org/10.1039/d0dt01587c.
[92] C. Chen, A. Wangriya, J.C. Buffet, D. O'Hare, Tuneable ultra high specific surface area Mg/Al-CO_3 layered double hydroxides, Dalton Trans. 44 (2015) 16392–16398, https://doi.org/10.1039/c5dt02641e.
[93] M.J. Climent, A. Corma, S. Iborra, K. Epping, A. Velty, Increasing the basicity and catalytic activity of hydrotalcites by different synthesis procedures, J. Catal. 225 (2004) 316–326, https://doi.org/10.1016/j.jcat.2004.04.027.
[94] M. Pavlovic, R. Huber, M. Adok-Sipiczki, C. Nardin, I. Szilagyi, Ion specific effects on the stability of layered double hydroxide colloids, Soft Matter. 12 (2016) 4024–4033, https://doi.org/10.1039/c5sm03023d.
[95] M.J. Climent, A. Corma, S. Iborra, A. Velty, Designing the adequate base solid catalyst with Lewis or Bronsted basic sites or with acid-base pairs, J. Mol. Catal. A Chem. 182–183 (2002) 327–342, https://doi.org/10.1016/S1381-1169(01)00501-5.